Chemosphere 244 (2020) 125488

Contents lists available at ScienceDirect

Chemosphere

journal homepage: www.elsevier.com/locate/chemosphere

High-throughput transcriptomics: An insight on the pathways affected in HepG2 cells exposed to nickel oxide nanoparticles

Quaiser Saquib [a, b, 1], Pu Xia [c, 1], Maqsood A. Siddiqui [b], Junjiang Zhang [c], Yuwei Xie [c], Mohammad Faisal [d], Sabiha M. Ansari [d], Hend A. Alwathnani [d], Abdulrahman A. Alatar [d], Abdulaziz A. Al-Khedhairy [a], Xiaowei Zhang [c, *]

[a] Zoology Department, College of Sciences, King Saud University, P.O. Box 2455, Riyadh, 11451, Saudi Arabia
[b] A.R. Al-Jeraisy Chair for DNA Research, Zoology Department, College of Sciences, King Saud University, P.O. Box 2455, Riyadh, 11451, Saudi Arabia
[c] State Key Laboratory of Pollution Control & Resource Reuse, School of the Environment, Nanjing University, Nanjing, 210023, PR China
[d] Department of Botany & Microbiology, College of Sciences, King Saud University, P.O Box 2455, Riyadh, 11451, Saudi Arabia

HIGHLIGHTS

- First report on transcriptome alterations in HepG2 by NiO-NPs exposure.
- NiO-NPs triggered hypoxia by up-regulation of *HIF-1α* and miR-210 in HepG2.
- NiO-NPs toxicity increased Ca^{++} influx, NO and $\Delta\Psi m$ in HepG2.
- NiO-NPs activated p53, p21, p16, MAPKPK2 proteins to induce cell death in HepG2.

ARTICLE INFO

Article history:
Received 12 September 2019
Received in revised form
24 November 2019
Accepted 26 November 2019
Available online 27 November 2019

Handling editor: Tamara S. Galloway

Keywords:
NiO-NPs
RNA-Seq
Toxicogenomics
Apoptosis
Transcriptome
Nanoparticles

ABSTRACT

Nickel oxide nanoparticles (NiO-NPs) have been used in several consumer goods, reported to demonstrate the hepatotoxic effects *in vitro* and *in vivo* test models. Nonetheless the molecular mechanism of hepatotoxicity is still missing. Hence, a toxicogenomic approach integrating microscopic techniques and high-throughput RNA sequencing (RNA-Seq) was applied to reveal hepatotoxicity in human hepatocellular carcinoma cells (HepG2). NiO-NPs induced a concentration dependent (5–100 μg/ml) cytotoxicity, with a No observed effect level (NOEL) of 5 μg/ml. Hypoxia-inducible transcription factor-1α (*HIF-1α*) and miR-210 microRNA were upregulated at 25 and 100 μg/ml, while significant alteration on transcriptome at mRNA and pathway level was observed at non-toxic level of NiO-NPs treatment. The treated cells also showed activation of glycolysis, glutathione, lysosomes and autophagy pathways by a pathway-driven analysis. Flow cytometric analysis affirmed the elevation in nitric oxide (NO), Ca^{++} influx, esterase, and disruption of mitochondrial membrane potential ($\Delta\Psi m$). Cell cycle dysregulation was affirmed by the appearance of 30.5% subG1 apoptotic peak in NiO-NPs (100 μg/ml) treated cells. The molecular responses were consistent with the microscopic observation that NiO-NPs induced subcellular alterations in HepG2 cells. We conclude that hypoxia stress played a pivotal role in NiO-NPs induced hepatoxicity in HepG2 cells. Concentration dependent effects on transcriptomics specify a powerful tool to evaluate the molecular mechanisms of nanoparticle induced cytotoxicity. Overall our study unequivocally affirmed the transcriptomic alterations in human cells, consequently the prevalent usage of NiO-NPs should be given subtle consideration owing to its effects on biological processes.

1. Introduction

Nickel oxide nanoparticles (NiO-NPs) is among front-runner nanomaterials (NMs) due to its unique physiochemical properties. Consequently, the industrial applications of NiO-NPs escalated rapidly in ceramics, electronics, catalysts, battery, biosensors,

* Corresponding author.
E-mail addresses: howard50003250@yahoo.com, zhangxw@nju.edu.cn (X. Zhang).
[1] These authors contributed equally to this work.

https://doi.org/10.1016/j.chemosphere.2019.125488
0045-6535/

electrochromic films, magnetic materials and diesel-fuel additive (Salimi et al., 2007; Rao and Sunandana, 2008; Mu et al., 2011). Despite the benefits that NPs own, scientists and regulators are keeping concerned about their potential environmental hazards and adverse effects on human health (Beaudrie et al., 2013). Especially the risk assessment of NMs on human health is far to be stated. The lack of epidemiological studies showing an association between NMs exposure and health effects, making toxicological studies mandatory to establish health consequences related to NMs exposure. Environmental contamination of coastal regions via production of NiO-NPs from welding fumes have been reported earlier (Wiesner et al., 2006). The involvement of Ni-NPs in catalysing the reversible hydration of CO_2 to carbonic acid led to its utilization to point flue sources like power plants and air-conditions outlets (Bhaduri and Siller, 2013).

NPs can reach bloodstream through inhalation, skin and through oral route via gastrointestinal tract (Muhlfeld et al., 2008; Korani et al., 2011; Schleh et al., 2012). Most of the *in vivo* studies on NiO-NPs have exhibited its pulmonary toxicities. BALB/c mice exposed to NiO-NPs exhibited lung injury, inflammation, increase in IL-6, 8-OHdG, caspase-3, with simultaneous decrease in IL-10 (Bai et al., 2018). Histological alterations and role of heme oxygenase 1 and nuclear factor erythroid 2-related factor 2 proteins have also been established as major cause for lung toxicity *in vivo* (Magaye et al., 2016). Irrespective of exposure route, liver is one of the prime target organs, exhibited high accumulation and retention of NPs (Hirn et al., 2011). In the same line, we have earlier reported the *in vivo* hepatotoxicity of NiO-NPs, triggering cell death and cytogenetic anomalies in the exposed rats (Saquib et al., 2017). NiO-NPs genotoxicity, chromosomal aberrations, DNA damage in lymphocytes, liver and kidney of female rats have also been reported (Dumala et al., 2017). Nickel nanoparticles (Ni-NPs) exposure resulted in testicular damage, oxidative damage, and apoptosis in rats (Kong et al., 2019). The life cycle study of earthworm (*Eisenia fetida*) reared in the presence of NiO-NPs revealed diminished reproductive capability, oxidative stress, DNA damage, and ultrastructural changes in the different tissues (Adeel et al., 2019). However, the underlying molecular and cellular mechanisms of NiO-NPs induced toxicities are largely unknown.

We have reported that NiO-NPs exposure resulted in ROS generation, DNA damage and activated the toxicity and some stress genes in HepG2 cells (Saquib et al., 2018). However, till date the most important query on NiO-NPs remain unanswered is what are the prominent network of vital signalling and metabolic pathways that can play prime role in its hepatotoxicity? That could lead to understand parallel consequences in exposed human populations and help regulatory bodies to define the NPs exposure limits. In addition, the critical toxicological information pertaining to NiO-NPs exposure and cellular uptake, its effect on mitochondrial functionality, role of Ca^{++} influx, activation of apoptotic proteins, cell cycle dysregulation and NO stress are still missing. Hence, there exists an urgent need to decipher how NiO-NPs affect the biological pathways at molecular and cellular level, especially at lower concentrations. Consequently, this study was aimed to apply the toxicogenomic approach incorporating microscopic techniques and high-throughput RNA sequencing (RNA-Seq) to assess the broad spectrum of cellular and molecular hazards in NiO-NPs exposed HepG2 cells.

2. Methods

2.1. NiO-NPs characterization, cell culture and NiO-NPs exposure

NiO-NPs were characterized by TEM, AFM, XRD and DLS, a detailed method for each analysis can be found in the supplementary file (supplementary information 1). HepG2 cells were cultured in DMEM supplemented with 10% fetal bovine serum (FBS), antibiotic-antimycotic solution (100x, 1 ml/100 ml of medium), and incubated at 37 °C in a humidified atmosphere containing 5% CO_2. As per the experimental need, 1×10^4/100 μl cells/well and 1×10^5 cells/ml were seeded in 96 and 6-well plates and allowed to attach with the surface for 24 h prior to NiO-NPs treatment. Considering the average daily intake of 150–168 μg nickel from food in USA, the low to high doses (5–100 μg/ml) were selected. The selected concentrations were intended to reflect the low level of potential human exposure, as well as probing the toxicological effects under accidental exposure with greater amounts of NiO-NPs (Report on Carcinogens Fourteenth Edition, 2011). Hence, for each set of experiment, NiO-NPs from low to high concentrations of NiO-NPs (5, 10, 25, 50 and 100 μg/ml) were ultra-sonicated for 15 min at 40 W and quickly added to culture wells to expose the cells for 24 h. Control groups were set as cells not exposed to NiO-NPs.

2.2. Cell viability

Cytotoxicity analysis was done using the commercially available kit (CellTiter 96 aqueous one solution assay kit, Promega, Madison, USA). Basic principal relying in this assay is to measure the metabolic activity of cells by adding the tetrazolium compound [3-(4,5-dimethylthiazol-2-yl)-5-(3-carboxymethoxyphenyl)-2-(4-sulfophenyl)-2H-tetrazolium, inner salt (MTS) and an electron coupling reagent phenazine ethosulfate (PES). MTS is reduced by the live cells to colored formazan by NADPH-dependent cellular oxidoreductase enzymes. Quantitation of formazan by measuring the absorbance at 490 nm is directly proportional to live cells in the culture medium. In brief, 20 μl per well CellTiter 96® aqueous one solution reagent was added into 96-well plate containing the untreated and NiO-NPs (5, 10, 25, 50 and 100 μg/ml) treated HepG2 cells. After incubation for 1 h at 37 °C, absorbance at 490 nm was measured in a Synergy H4 Hybrid Multi-Mode Microplate reader (BioTek Instruments, Winooski, VT). For neutral red uptake (NRU) assay 50 μg/ml of neutral red dye was added to the untreated and treated cells and incubated for 3 h. Medium was washed off rapidly with a solution containing 0.5% formaldehyde and 1% calcium chloride and incubated for 20 min at 37 °C in a mixture of acetic acid (1%) and ethanol (50%). At the end of incubation period, the aqueous medium was carefully aspirated and 200 μl of DMSO was added to each well and absorbance was read on a microplate reader at 550 nm (Saquib et al., 2016).

2.3. High-throughput RNA sequencing (RNA-Seq) and data analysis

For the transcriptomic studies, HepG2 cells were treated with non-cytotoxic (5 μg/ml), medium-cytotoxic (25 μg/ml) and cytotoxic (100 μg/ml) concentrations of NiO-NPs for 24 h at 37 °C in CO_2 incubator. For each experiment, triplicate assays were performed in three batches of culture cells. HepG2 cells were harvested after 24 h of exposure, and subjected to total RNA isolation using RNeasy mini kit (QIANGEN, GmbH, Hilden), all RNA samples were stored at −80 °C until use. The RNA concentrations were measured and its quality was determined using Agilent 2100 bioanalyzer (Angilent technologies, Santa Clara, CA, US). For each triplicate assay, replicate RNA samples of same concentration treatment were pooled and submit to prepare RNA libraries. Total 12 libraries were prepared from 4 μg of total RNA using Dynabeads mRNA DIRECT Micro Kit (Life technologies, AS, Oslo, Norway) and Ion Total RNA-Seq Kit v2 (Life technologies, Austin). Sequencing was performed on Ion Torrent Proton with Ion PI Template OT2 200 Kit v3 (Life technologies, Carlsbad, CA, USA) and Ion PI Sequencing 200 Kit v3 (Life

technologies, Carlsbad, CA, USA) following the manufacturer's protocol.

Raw sequences were mapped to full genome sequences for *Homo sapiens* (UCSC version hg19) using the Torrent Mapping Alignment Program (TMAP). Aligned bam files were downloaded and delivered to GenomicAlignments (Bioconductor version 1.2.1) (Lawrence et al., 2013) for counting reads mapped to each gene, based on database TxDb.Hsapiens.UCSC.hg19. knownGene (Bioconductor version 3.0.0). Counted reads were analysed for differential expression of genes using DESeq2 (Bioconductor version 1.6.2) (Love et al., 2014). Genes that were significantly demonstrated differential expression (DGE) were selected as adjusted $p < 0.05$ and fold-change ≥ 1.5 or ≤ 0.667. Pathway analysis was conducted with gage (Bioconductor R package, version 2.16.0) and pathview (Bioconductor R package, version 1.6.0). Gene set enrichment analysis was conducted to gain enriched gene ontologies (GO) terms and Kyoto Encyclopedia of Genes and Genomes (KEGG) pathways. At last, we selected several RNA-Seq DEGs for qPCR-PCR validation (Supplementary Table 1).

2.4. NiO-NPs translocation in HepG2 cells

NiO-NPs translocation in HepG2 cells was analysed using TEM. In brief, cell pellets from control and NiO-NPs (100 μg/ml) treatment group was fixed in glutaraldehyde for 10 min followed by resuspension of cells in OsO_4 (1%) for 1 h at 4 °C. An additional incubation of 1 h was given for each cell suspension in 2% aqueous uranyl acetate pursued by the dehydration of cells using ascending grade of ethanol. Cells were finally embedded in low viscosity araldite resin and ultrathin sections of 80 nm were made for TEM analysis under high vacuum (100 kV) (Saquib et al., 2013).

2.5. $\Delta\Psi m$ measurements in HepG2 cells

Qualitative analysis of $\Delta\Psi m$ in NiO-NPs treated cells grown on glass chamber slides, were done by staining cells with 20 μM of Rh123 for 60 min at 37 °C in CO_2 incubator. Fluorescence images were captured on microscope equipped with fluorescent lamp (Nikon Eclipse 80i, Japan). Quantitative analysis of $\Delta\Psi m$ was done in NiO-NPs treated cells following our previously described method (Saquib et al., 2013). In brief, cells were trypsinized, pelleted and washed twice with cold PBS, followed by the resuspension of cells separately in 500 μl PBS (Ca^{++} and Mg^{++} free) containing Rh123 (5 μg/ml). All cells were incubated for 60 min at 37 °C in dark followed by washing and the fluorescence were recorded upon excitation at 488 nm at FL1 Log channel through 525 nm band-pass filter on Beckman Coulter flow cytometer (Coulter Epics XL/Xl-MCL, USA).

2.6. NO, Ca^{++} and esterase quantification

Intracellular NO, Ca^{++} influx and esterase activities in HepG2 cells were measured using flow cytometry. In brief, untreated and NiO-NPs treated cells were trypsinized and pelleted at 3000 rpm for 5 min. All pellets were washed twice with cold PBS and incubated separately with NO specific 4,5-diaminofluorescein diacetate (DAF2-DA) (5 μM), Ca^{++} specific Fluo-3 (4 μM) and esterase specific carboxyfluorescein diacetate succinimidyl ester (CFDA-SE) (5 μM) dyes for 60 min at 37 °C in CO_2 incubator. After staining, cells were spin down at 3000 rpm for 5 min, followed by two successive washes with PBS. The cells were resuspended in a final volume of 500 μl of PBS and the fluorescence of DAF2-DA, Fluo-3 and CFDA-SE were measured in 10000 cells at log scale (FL-1, 530 nm) using flow cytometer.

2.7. Cell cycle analysis

HepG2 cells treated with varying concentrations (25, 50 and 100 μg/ml) of NiO-NPs for 24 h were detached and processed for cell cycle analysis. Cells were fixed with 500 μl of chilled 70% ethanol and incubated at 4 °C for 1 h. After washing, cell pellets were resuspended in 500 μl PBS containing propiodium iodide (50 μg/ml) dye, 0.1% Triton X-100 and 0.5 mg/ml RNAase A. The fluorescence of 10000 events of propiodium iodide stained cells were acquired at laser excitation of 488 nm and 620 nm band-pass filter using flow cytometer. Data were analysed by excluding the cell debris, characterized by a low FSC/SSC using Beckman Coulter flow cytometer (Coulter Epics XL/Xl-MCL, USA and System II Software, Version 3.0) (Saquib et al., 2013).

2.8. Immunofluorescence and western blotting analysis

HepG2 cells were exposed to 100 μg/ml of NiO-NPs in 16 well Nunc glass chamber slides for 24 h. Cells were incubated with primary antibodies (anti-p53, anti-bax, anti-bcl2, anti-PARP and anti-MAPKPK2) at dilution of 1:50. Secondary antibody (goat anti-rabbit IgG-FITC) at a dilution of 1:100 was used to stain the primary antibodies. Detailed methodology of immunofluorescence can be found in the supplementary file (supplementary information 1).

For the western blotting, lysis of control and NiO-NPs (100 μg/ml) treated cells were done using 1x SDS buffer (62.5 mM Tris—HCl, 2% SDS, 10% glycerol, 50 mM DTT) supplemented with protease inhibitors and phosphatase. Equal amount of proteins (15 μg/well) were loaded on 10% SDS-polyacrylamide gels, separated electrophoretically and transferred on Immun-blot PVDF membrane and processed for blocking and incubation with anti-p21, anti-p16, anti-caspase-3, anti-caspase-8, anti-caspase 9 and anti-GAPDH antibodies. Detailed methodology of western blotting can be found in the supplementary file (supplementary information 1).

2.9. Statistical analysis

Statistical analysis was done by one-way ANOVA (Dunnett's multiple comparisons test) using Sigma Plot 11.0, USA. The level of statistical significance chosen was $p < 0.05$, unless otherwise stated.

3. Results

3.1. Cytotoxicity and NiO-NPs characterization

Substantial reduction of 18%, 29%, 41%, and 61% in HepG2 survival was observed at 10, 25, 50 and 100 μg/ml of NiO-NPs after 24 h of exposure (Fig. 1a). No apparent evidence of cytotoxicity was noticed at low concentration of 5 μg/ml.

The size of NiO-NPs under study was 21.6 ± 3.6 nm by TEM, 30 ± 1.4 nm by AFM, 20.3 nm by XRD analysis. DLS data showed large particle aggregates of 346 ± 3.2 nm of NiO-NPs in water and 197 ± 2.8 nm in DMEM cell culture medium, refer to supplementary file (Supplementary Figs. 1a—d). NRU assay also showed a concentration dependent cytotoxicity in HepG2 cells at 25, 50 and 100 μg/ml NiO-NPs induced 7.4%, 14.8% and 18.4% decline in the cell viability, refer to supplementary file (Supplementary Fig. 2a). The morphological analysis of NiO-NPs treated cells explicitly demonstrated the toxicity, manifested as detachment of the adherent cells at increasing concentrations of NiO-NPs, refer to supplementary file (Supplementary Fig. 2b). Cytotoxic effects of $NiNO_3$ were also determined to illustrate the effects of solubilized Ni^{++} ions in HepG2 cells. The cytotoxicity assays did not showed reduction in cell viability with $NiNO_3$ at the tested concentrations, refer to supplementary file (Supplementary Fig. 3).

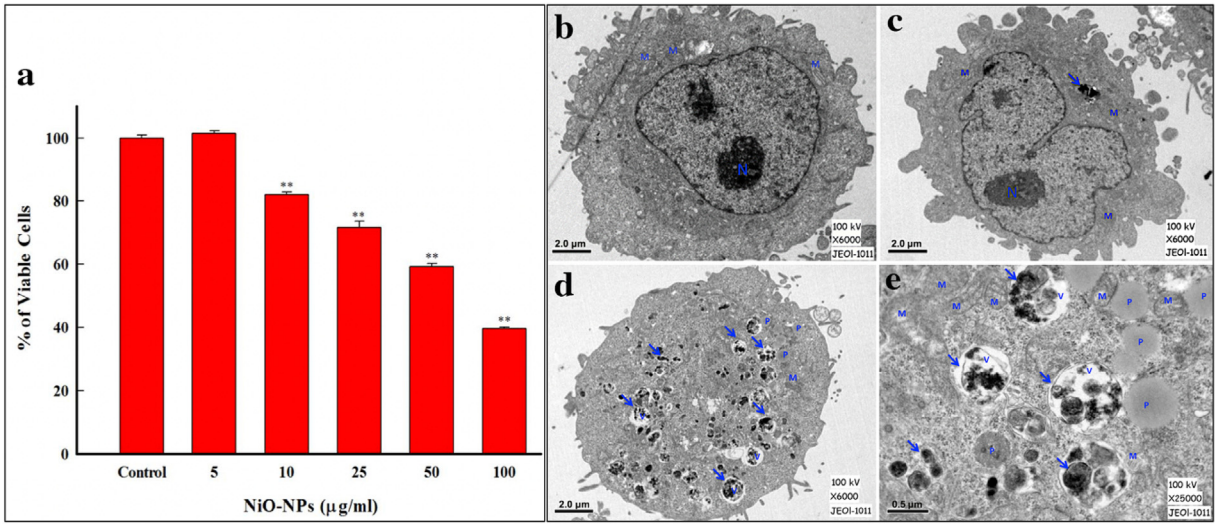

Fig. 1. Effect of NiO-NPs on HepG2 survival and ultrastructural changes. (a) Cell survival assay showing concentration dependent reduction in HepG2 cells exposed to NiO-NPs. (b) Ultrastructural analysis of untreated (control) HepG2 cells. (c, d) NiO-NPs (100 µg/ml) treated HepG2 cells showing NPs aggregates in vacuoles. (e) Magnified image of panel (d) showing mitochondria with damaged cristae and increased number of peroxisomes. N; nucleus, M; mitochondria, V; vacuoles, P; peroxisomes.

3.2. Translocation of NiO-NPs in HepG2 cells

Ultrastructural analysis revealed that NiO-NPs were translocated in the cytoplasm and induces subcellular changes in HepG2 cells. NiO-NPs in cells were identified as an aggregate entrapped in vacuoles. The treated cells also showed increased number of peroxisomes and degenerated mitochondria. However, no such changes were observed in the untreated control cells (Fig. 1b–e).

3.3. Transcriptome alteration and functional enrichment analysis

The RNA-Seq detected 12400 to 13929 genes (reads>5) aligned to human genome in total 12 libraries. The number of differentially expressed genes (DEGs) increased with the concentration level from non-cytotoxic (5 µg/ml) to medium (25 µg/ml) to high cytotoxic (100 µg/ml) (Fig. 2a and b). The profiling of top 53 DEGs also showed a dose-dependent trend. Only six genes, micro RNA host

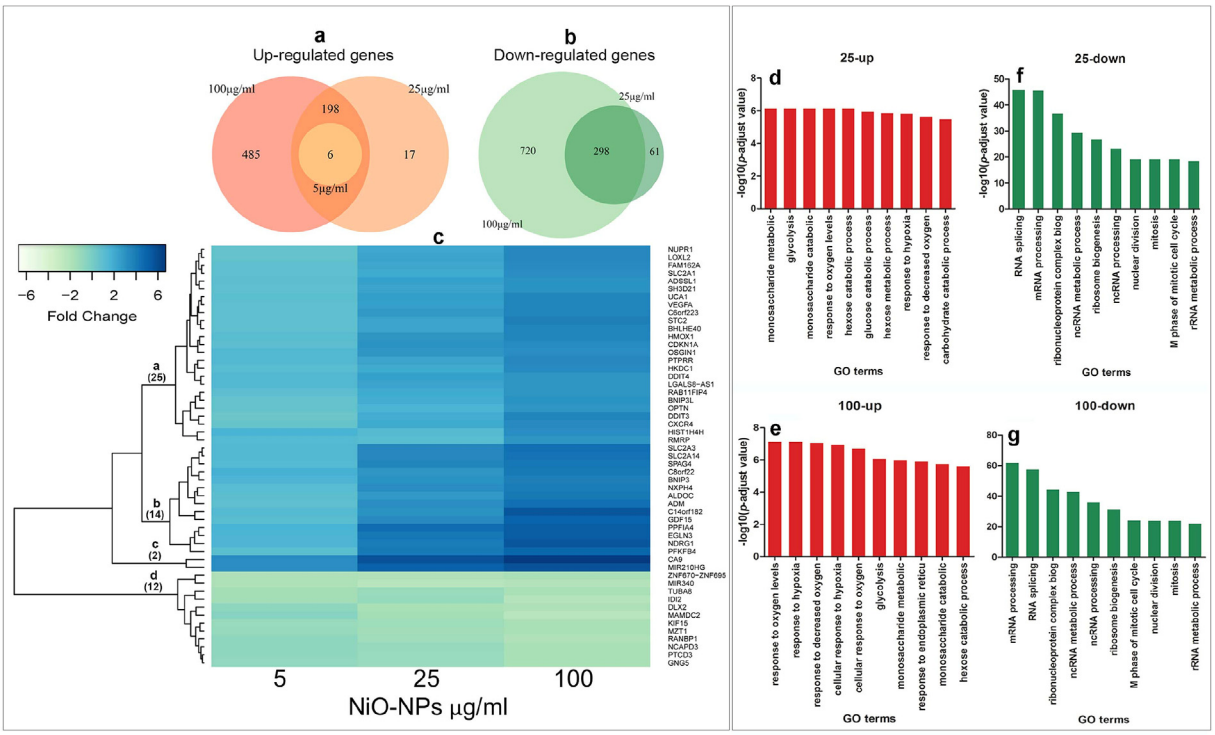

Fig. 2. Transcriptomic alterations in HepG2 cells treated by NiO-NPs. Venn diagram comparison of NiO-NPs treatment in HepG2 cells (a) Up-regulated genes and (b) Down-regulated genes in treated cells. 5, 25 and 100 µg/ml indicate the low, medium and high cytotoxic concentrations of NiO-NPs. The number in overlapped area represents the overlapping genes. (c) Heat map of top 53 differentially expressed genes significantly altered in 5, 25 and 100 µg/ml of NiO-NPs treated groups. Top 10 GO terms enriched by up-regulated and down-regulated genes in the NiO-NPs (25 and 100 µg/ml) treated HepG2 cells. In each plot, the GO terms were aligned from left to right according to their *p* values from low to high. (d and e) Up-regulated GO terms at 25 and 100 µg/ml (f and g) down-regulated GO terms at 25 and 100 µg/ml.

gene (*miR-210 HG*), carbonic anhydrase 9 (*CA9*), solute carrier family 2 member 3 (*SLC2A3*), BCL2 interacting protein 3 (*BNIP3*), Egl nine homolog 3 (*EGLN3*) and N-Myc downstream regulated 1 (*NDRG1*), were differentially expressed (up-regulated) at 5 μg/ml, and these genes were also among the top of differentially expressed (up-regulated) genes at 25 and 100 μg/ml concentrations (Fig. 2c). For 25 and 100 μg/ml of NiO-NPs, top 10 up-regulated GO terms were mainly involved with hypoxia stress response (i.e., cellular response to oxygen levels and cellular response to hypoxia) (Fig. 2d and e) and top 10 down-regulated GO terms were mainly related with basic cellular processes (i.e., RNA splicing and nuclear division) (Fig. 2f and g). While no GO terms were substantially enriched at 5 μg/ml of NiO-NPs. The top enriched GO terms of biological processes for 25 and 100 μg/ml of NiO-NPs treatments were related with glucose metabolism (i.e., glycolysis, hexose catabolic process).

In addition to GO terms, we investigated the up-regulated and

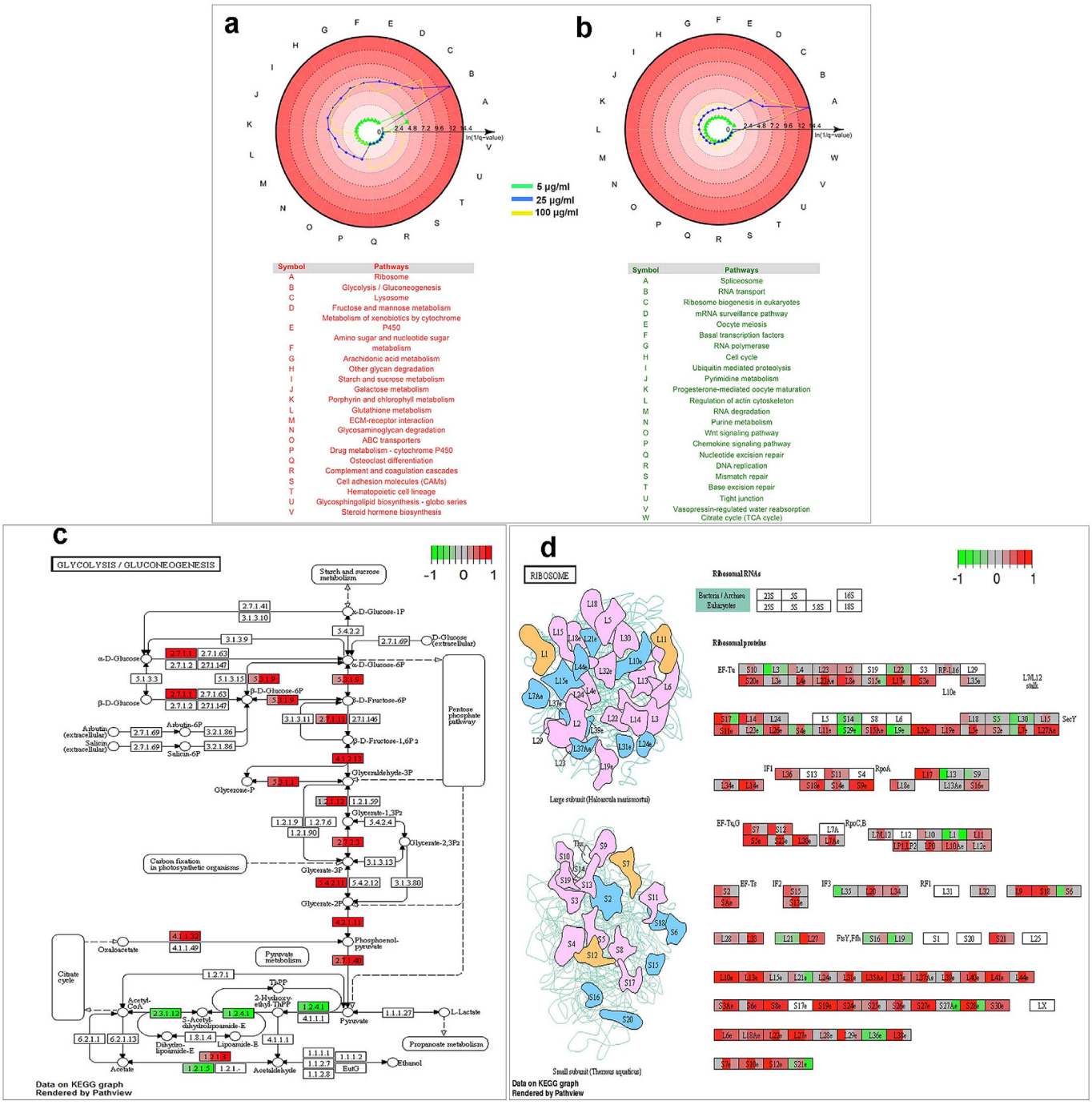

Fig. 3. Enriched KEGG pathways following exposure of HepG2 to 5, 25 and 100 μg/mL of NiO-NPs. (a) Significantly up-regulated and (b) down-regulated KEGG pathways showing different directions represent varying enriched pathways. The significance of each pathway was represented as distance between dot and circle centre (ln (1/q-value)). (c) Significantly enriched gene network of glycolysis/gluconeogenesis and (d) Expression profiles of genes involved in enriched "ribosome" term after NiO-NPs-treated HepG2 cells. The genes in red and green refer to the up-regulated and down regulated genes. Abbreviations for the KEGG parameters can be found on the KEGG pathway webpage. (For interpretation of the references to color in this figure legend, the reader is referred to the Web version of this article.)

down-regulated KEGG pathways. It is showed that the top up-regulated KEGG pathways for 25 and 100 μg/ml were related with glucose metabolism (i.e., glycolysis, hexose catabolic process) (Fig. 3a, c). Pathway related with ribosome was considerably up-regulated at 5 μg/ml, but down-regulated at 25 and 100 μg/ml of NiO-NPs (Fig. 3a and b). Concurrently, the most substantial enriched KEGG pathway was ribosome (Fig. 3d). Moreover, nucleotide excision repair (NER), base excision repair (BER) and mismatch repair (MR) systems were essentially down-regulated (Fig. 3b). The down-regulation of ubiquitin mediated proteolysis pathways at 100 μg/ml suggested a disruption of protein biosynthesis (Fig. 4). The mRNA expression of eight candidate genes in three concentrations was validated as compared to RNA-Seq and qPCR (Fig. 5a). Results showed that apoptotic gene caspase 4 (*CASP4*), glycolysis related gene pyruvate kinase muscle isozymes (*PKM*) and the *HIF-1α* related genes *CA9*, *SLC2A3*, *BNIP3*, *EGLN3*, *GSTA4* and *NDRG1* were upregulated and dose-dependent (Fig. 5b). Substantial expression of miR-210 was validated as compared to control. Results showed that the expression of miR-210 was dose-dependent to NiO-NPs exposure (Fig. 5c).

3.4. Dysfunction of mitochondrial membrane potential ($\Delta\Psi m$)

HepG2 cells treated with increasing concentrations of NiO-NPs showed prominent shift of Rh123 fluorescence peaks towards greater logarithmic scale (Fig. 6a). After 24 h of incubation, cells exposed to 25, 50 and 100 μg/ml exhibited 121%, 124% and 128% ($p < 0.01$) increase in $\Delta\Psi m$ over control (Fig. 6a, Inset). The fluorescence microscopic images of NiO-NPs treated cells reaffirmed the enhancement of Rh123 fluorescence (Fig. 6b).

3.5. Quantitation of intracellular NO, Ca^{++}, esterase and cell cycle

NiO-NPs treated HepG2 cells exhibited an increase in intracellular NO generation. Relative to 100% fluorescence of DAF2-DA in control, the treated cells showed 128.9%, 124.8% and 122.1% ($p < 0.01$) higher fluorescence at 25, 50 and 100 μg/ml of NiO-NPs (Fig. 7a). Ca^{++} influx in the treated cells was analysed using Fluo-3. NiO-NPs (50 and 100 μg/ml) treated groups exhibited 456.9% and 474.6% increased Fluo-3 fluorescence. In contrast, no change in Fluo-3 fluorescence was observed in cells treated with 25 μg/ml (Fig. 7b). Esterase analysis by CFDA-SE dye also revealed an enhanced level of esterases activity in NiO-NPs treated groups. Compared to 100% fluorescence in control, NiO-NPs (25, 50 and 100 μg/ml) treatments resulted in 124.6%, 125.8% and 128.7% higher fluorescence of CFDA (Fig. 7c). The representative cell cycle images exhibit a concentration dependent apoptosis induction in NiO-NPs treated cells (Fig. 7d). Quantitative analysis of cell cycle showed that NiO-NPs (25, 50 and 100 μg/ml) treatment for 24 h induced 11.0 ± 2.6, 19.0 ± 1.7 and 30.5 ± 2.5%) increase in subG1 apoptotic peak in HepG2 cells (Fig. 7e).

3.6. Immunofluorescence and western blotting

The fluorescent signal of apoptotic proteins (p53 and bax) in HepG2 cells exposed to 100 μg/ml of NiO-NPs was considerably high in the cytoplasm. While, the fluorescence of anti-apoptotic protein (bcl2) was lower. Apart from the cytoplasmic localization of p53, bax and bcl2, these proteins were also found localized on the nucleolus of the treated cells (Fig. 7f). Nonetheless, fluorescence signals of MAPKPK2, cyto c and PARP in NiO-NPs treated cells showed cytoplasmic localization, and the intensity of fluorescence was fairly consistent throughout a cell population. However, nucleolar localization of these proteins was not observed. Western blotting data showed that the translation expression of p21 and p16 proteins was elevated upon NiO-NPs (100 μg/ml) exposure. On the other hand, levels of caspases-3, 8 and 9 were also increased, as compared to the control (Fig. 7g).

4. Discussion

Here in, we provide first evidence on NiO-NPs induced alterations in HepG2 transcriptome at mRNA and pathway level. In RNA-Seq experiments, the *HIF-1α* target genes were consistently over-expressed from 5, 25 and 100 μg/ml of NiO-NPs, suggesting that hypoxia stress response pathway played a vital role in NiO-NPs toxicity. A single study on NiO-NPs also exhibited hypoxia stress in human fetal lung fibroblasts cells (Qian et al., 2015). Nickel compounds could mimic hypoxia via impairing the ascorbate and inactivate prolyl hydroxylases, resulting the stabilization of *HIF-1α* and expression of *HIF-1α* target genes (Pietruska et al., 2011). At 5 μg/ml, we found that *miR210 HG*, a host gene of microRNA 210 (miR-210) was most up-regulated among six genes (*miR210 HG*, *CA9*, *SLC2A3*, *BNIP3*, *EGLN3* and *NDRG1*). Previous studies have reported that miR-210 is a signature of hypoxia (Valera et al., 2011). In fact, the detected transcript of *miRNA210 HG* was miR-210 precursors with poly-A tails, whereas a mature miR-210 does not contain poly-A tails (Lee et al., 2004). In addition to *miR210 HG*, other 5 genes (*CA9*, *SLC2A3*, *BNIP3*, *EGLN3* and *NDRG1*) were consistently overexpressed, and are all *HIF-1α* target genes. It is well accepted that *CA9* and *SLC2A3* are involved in the hypoxia-induced glucose metabolism (Benej et al., 2014), and *BNIP3*, *EGLN3* and *NDRG1* are correlated with hypoxia-induced cell death (Han et al., 2014). *SLC2A3* encodes glucose transporter 3 (*GLUT3*) functions as a glucose transporter in cells (Simpson et al., 2008).

Down-regulation of ribosome biogenesis pathway was observed

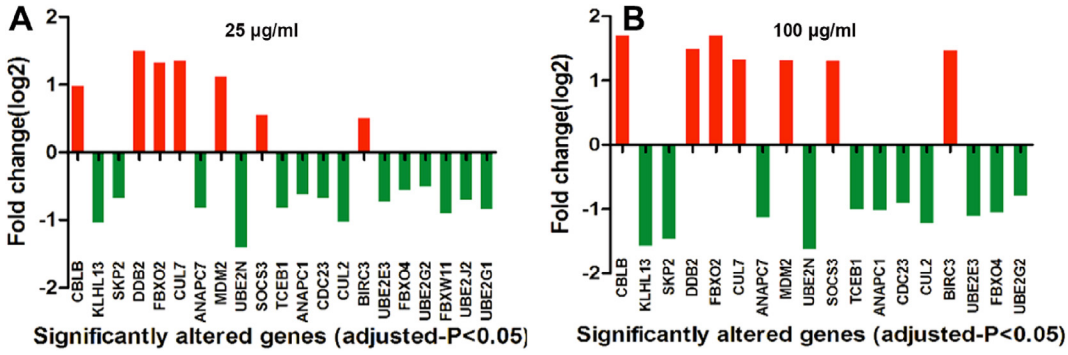

Fig. 4. Substantially altered genes involved in ubiquitin mediated proteolysis pathway at 25 μg/ml and (D) 100 μg/ml. Red and green histograms denote up-regulation and down-regulation of genes. (For interpretation of the references to color in this figure legend, the reader is referred to the Web version of this article.)

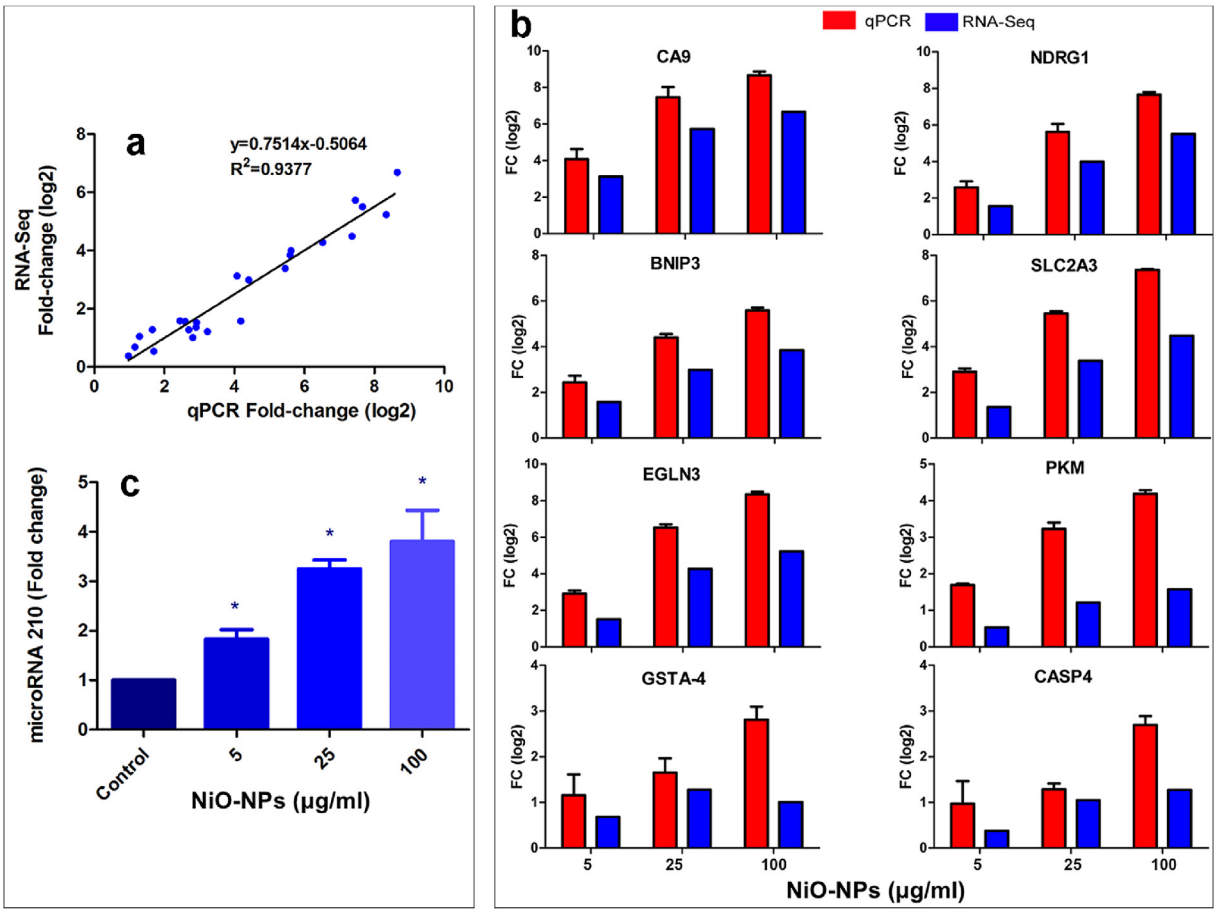

Fig. 5. Validation of RNA-Seq experiments. (a) Comparison of fold-change (log 2) values between RNA-Seq and qPCR, showing linear and significant ($p<0.0001$; $r^2 = 0.94$). (b) micro RNA qRT-PCR validation of miR-210 in HepG2 cells exposed to different concentrations of NiO- NPs. (c) Relative expression ratios of selected genes determined by RNA-Seq and qPCR analysis. Data represented are mean ± standard deviation (s.d.) of three identical experiments made in three biological replicate ($^*p < 0.05$ vs. control).

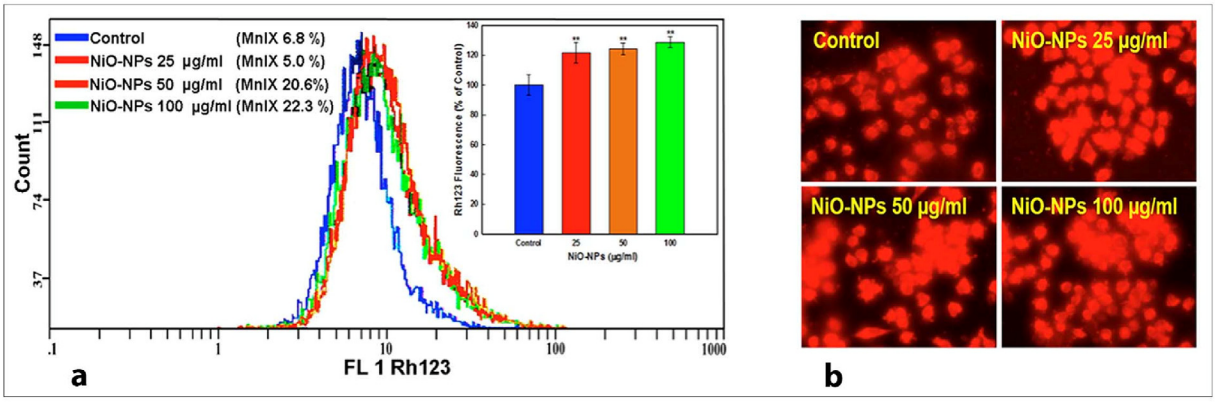

Fig. 6. Effect of NiO-NPs on HepG2 mitochondrial membrane potential. **(a)** Flow cytometric measurements of $\Delta\Psi m$ in treated cells indicating enhancement of rhodamine 123 (Rh123) fluorescence. Each histogram in inset represents the values of mean ± SD of three independent experiments done in triplicate wells. ($^{**}p < 0.01$ vs. control). MnIX; mean intensity. **(b)** Fluorescence microscopic images of treated cells showing an enhancement of Rh123 fluorescence.

in HepG2 cells treated with 25 and 100 µg/ml of NiO-NPs, which might be the cellular defence response to hypoxia stress. Loss of functional attributes of genes involved in ribosome biogenesis has been linked with tolerance to hypoxia (Shah et al., 2011). *GSTA4* and *IDH2* genes are critically important for the mitochondrial antioxidant enzyme showed considerable up-regulation (Sebastian and Mostoslavsky, 2010), indicated an early oxidative and antioxidant activity in mitochondria. Cell cycle pathway was down-regulated at 25 and 100 µg/ml, suggesting cell cycle arrest by *ORC6, ANAPC7* and *CCNA2* genes. However, we did not encounter cell cycle arrest, although we suggest that the expression of *ORC6, ANAPC7* and *CCNA2* genes could be for a transient phase and cell enters the apoptotic stage directly, refer to supplementary file (Supplementary Fig. 4a).

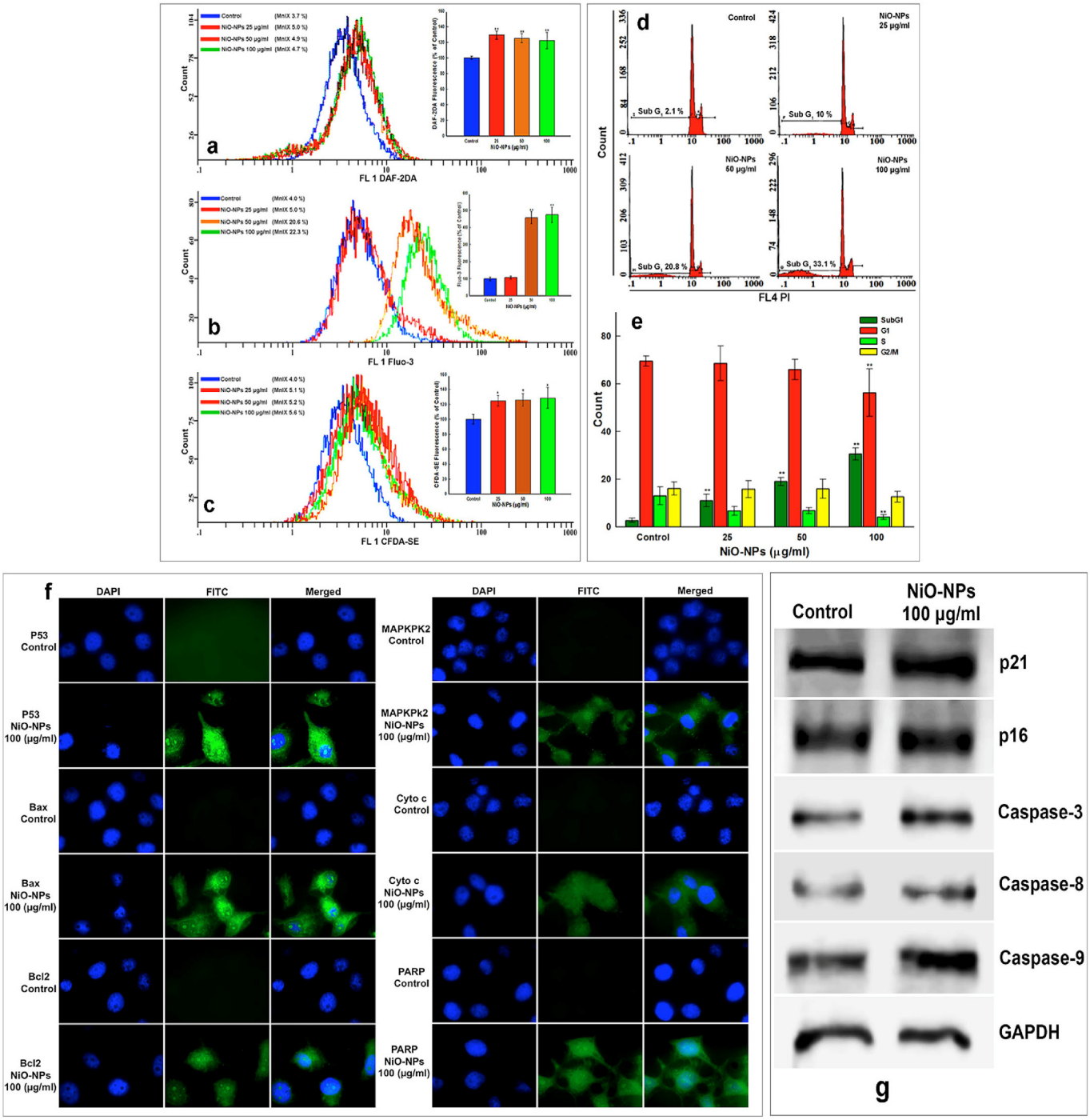

Fig. 7. Elevation of NO level and Ca^{++}, cell cycle dysregulation and activation of apoptotic proteins by NiO-NPs exposure. **(a)** Flow cytometric analysis of intracellular NO, **(b)** Ca^{++} influx and **(c)** esterase level in NiO-NPs treated HepG2. Each histogram in inset represents the values of mean ± SD of three independent experiments done in triplicate wells ($^{*}p < 0.05$, $^{**}p < 0.01$ vs. control). **(d)** Representative flow cytometric images showing NiO-NPs induced increase of apoptotic (subG1) peak **(e)** Different phases of cell cycle obtained from three independent experiments in triplicate wells (mean ± SD, $^{**}p < 0.01$ vs. control). **(f)** Immunofluorescence images and **(g)** western blots of apoptotic proteins activated in HepG2 cells after NiO-NPs (100 µg/ml) treatment for 24 h.

Autophagy and apoptosis are usually activated together when cells are under stress condition. We found that genes involved in phagosome formation and lysosomes pathways were altered at 25 and 100 µg/ml, refer to supplementary file (Supplementary Figs. 4b and c), indicating greater formation of autophagosomes. Previous study has also linked the induction of autophagy and cell death by NPs (Johnson et al., 2015). Moreover, *BNIP3* has been reported to play a vital role in autophagy induced by hypoxia (Tracy and Macleod, 2007). Considering the activation of *BNIP3* in RNA-Seq, we also suspect its possible role in mitochondrial fragmentation as well as autophagy via *BNIP3* dimers formation, which can cause damage to the mitochondria. Alternatively, *BNIP3* may also act as "mitochondrial quality control" by ridding out damaged mitochondria by targeting them to the autophagosomes for

degradation. In fact, we did not measure the autophagy in HepG2 cells, however, these correlations warrant an in-depth investigation to establish a concrete link between *BNIP3* and mitochondrial damage. Repression of spliceosome genes was also observed in NiO-NPs exposed HepG2 cells (Fig. 8), which strongly pointed towards its erroneous dual function in recognizing the intron/exon boundaries and catalysing the cut-and-paste reactions that remove introns and join exons in mRNA. It has been reported that the suppression of splicing machinery may result in DNA damage, cell cycle arrest and apoptosis (Bonassi et al., 2007; Trouiller et al., 2009; Tiwari et al., 2011; Karamysheva et al., 2015), which is clearly evident in the NiO-NPs treated HepG2 cells.

The ultrastructural results showed severe vacuolization in HepG2 cells containing NPs aggregates, degenerated mitochondria

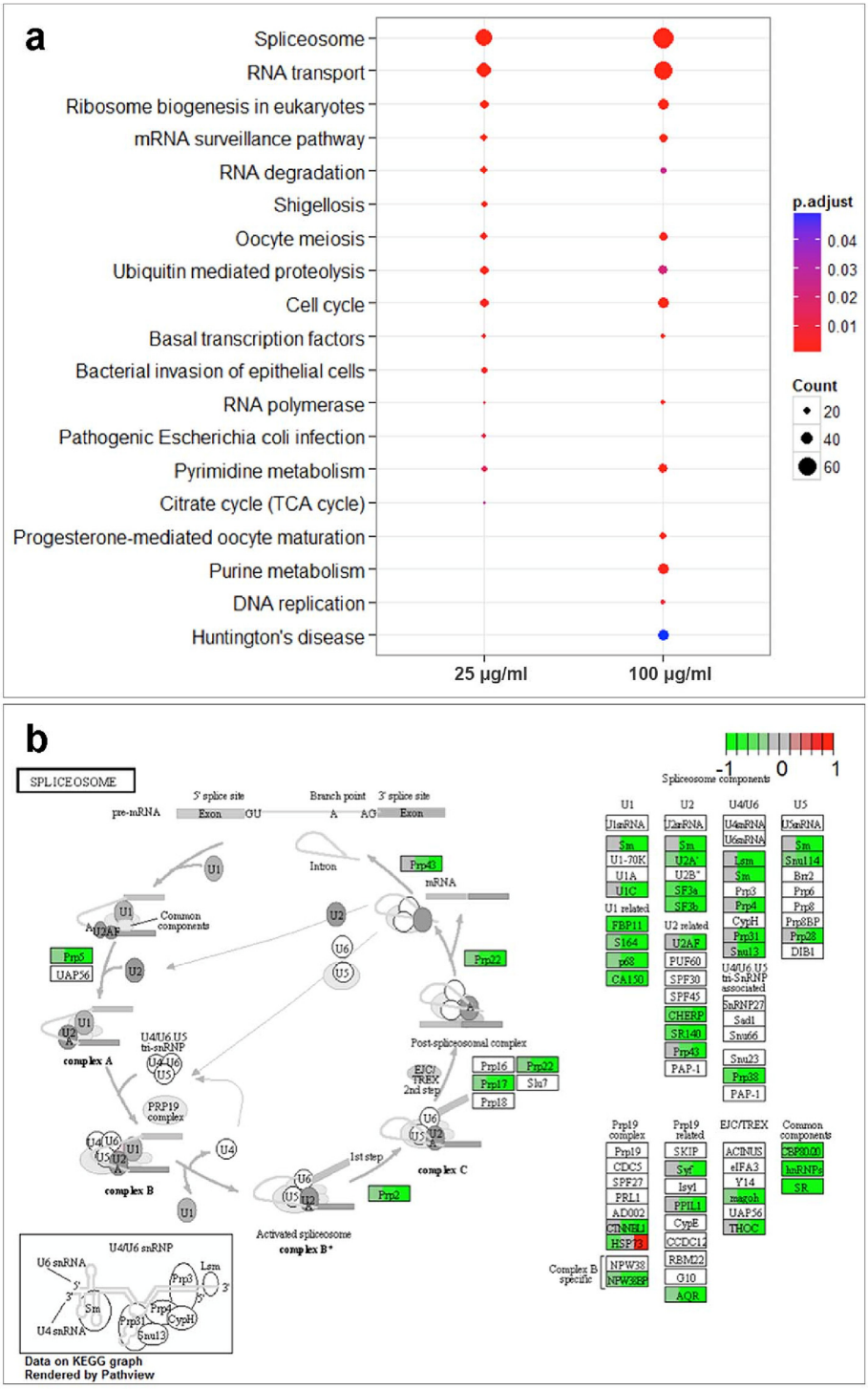

Fig. 8. Enrichment of spliceosome pathways in HepG2 cells. (a) Significantly enriched KEGG terms and (b) Spliceosome KEGG pathway in NiO-NPs treated HepG2 cells. Red and green boxes represent up-regulated and down-regulated genes in the treated cells. Significant differences from the control are indicated by $^{*}p < 0.05$. (For interpretation of the references to color in this figure legend, the reader is referred to the Web version of this article.)

with abundance of peroxisomes. Peroxisome biogenesis as a consequence of mitochondrial dysfunction has been observed in yeast (Epstein et al., 2001). In addition, the lysosomal destabilization is regarded as a prior event of mitochondrial injury during chemically induced apoptosis (Zhao et al., 2003). Mitochondrial dysfunction in HepG2 cells corresponded with our recent report on mitochondrial damage in rat bone marrow cells orally exposed to NiO-NPs (Saquib et al., 2017). An enhanced fluorescence of Rh123 in HepG2 can be related with the mitochondrial property to swell under overwhelming conditions like Ca^{++} influx, pH and cytochrome *c* release during apoptotic cell death (Saquib et al., 2016). We have found an enhanced level of NO in NiO-NPs treated cells, which corroborate with overall ROS generation in NiO-NPs treated HepG2 cells (Saquib et al., 2018). Albeit, we suggest the selective role of NO in NiO-NPs induced oxidative stress. NO has also been associated with the collapse of $\Delta\Psi m$, as well as impairing the mitochondrial ATP synthesis to trigger cell death (Almeida and Bolanos, 2001). An increase in Ca^{++} influx was observed in NiO-NPs treated cells. In addition to the free cytoplasmic Ca^{++}, the level of mitochondrial Ca^{++} has also been implicated in apoptosis induction (Rasola and Bernardi, 2011). NO play an additive role in releasing Ca^{++} from mitochondria and thereby causes mitochondrial destabilization (Richter and Kass, 1991). NO or more likely the reactive products derived from it, such as $NO_2\cdot$, $ONOO^-$, N_2O_3 and HNO_2 have the potential to produce nitration, nitrosation and deamination reactions on DNA (Wiseman and Halliwell, 1996). Hence, the possible impairment of DNA repair machinery resulted in HepG2 cell death, as also evident by the appearance of sub G1 apoptotic peak in the cell cycle data.

Western blotting data showed an elevated level of p21 and p16 proteins in NiO-NPs treated cells. The data is in accordance with increased activity of both proteins (p21 and p16) in nanoceria exposed murine neuronal cells, and regarded as apoptotic cell death promoter depending on particular cellular stresses and stimuli (Lee et al., 2012; Mirzayans et al., 2012). The enhanced cytoplasmic localization of p53, bax, bcl2, MAPKPK2, cyto c and PARP in immunofluorescence data indicated the translational activation of apoptotic proteins as a consequence of NiO-NPs treatment. During DNA damage, p53 is activated and translocated to the nucleus, where it can induce pro apoptotic gene expression and accelerate the cell death process (Sheikh and Fornace, 2000). Mitochondrial dysfunction plays a crucial role in apoptosis, particularly the bcl2 family members (bax and bcl2) are the key factors in mitochondrial-dependent apoptotic cell death. An enhanced NO production, as observed above, can also react in a diffusion-controlled process to produce peroxynitrite ($ONOO^-$), known to interact with mitochondria and trigger apoptotic cell death (Murphy, 1999; Saquib et al., 2016). Although, we did not quantitate the $ONOO^-$, but we postulate that it may interfered with the mitochondrial function and elevated the Ca^{++}, which possibly activated NO mediated apoptosis in HepG2 cells. NiO-NPs exposed cells have also showed an increased expression of bax and low expression of bcl2 proteins. In this line, NO mediated apoptosis has been implicated to severely affect the recruitment of regulatory apoptotic proteins (bax, bcl2) to the outer membrane of mitochondria or affecting their relative amounts (Murphy, 1999). We observed a conspicuous nucleolar localization of p53, bax and bcl2 in HepG2 cells. It is proposed that nucleolus functions as a sensor that monitors the strength of cellular stress by regulating p53 acetylation in nucleolus, which trigger apoptosis by regulating the degree of rRNA transcription and perturb ribosome biogenesis (Kruger and Scheer, 2010). Hence, we suggest that p53 nucleolar localization may also share the similar mechanism to inhibit ribosome biogenesis in HepG2 cells, as also validated by the RNA-Seq experiments.

Additionally, the nucleolar localization of bax indicates a general response of DNA damage (Joy et al., 2000). NiO-NPs activated the MAPK pathway ultimately leading to apoptosis in the HepG2 cells. Consistent with our results, cerium oxide-NPs have been reported to induce apoptosis in SMMC-7721 cells via MAPK signalling (Cheng et al., 2013). The translational upregulation of p53, as observed in immunofluorescence data, entails the impairment of cellular repair machinery, leading to the initiation of apoptotic process to prevent subsequent passage of mutations to other cells. On the other hand, we found dysfunction of $\Delta\Psi m$, which has considerable importance as an early apoptotic event. The main intrinsic pathway is characterized by mitochondrial dysfunction, with the release of cytochrome *c* and activation of caspases (Porter and Janicke, 1999).

In conclusion, NiO-NPs prompted severe hypoxia and disrupting the glycolysis and ribosome biogenesis pathways, affirming its potential hepatotoxic effects. NiO-NPs caused a concentration dependent cytotoxicity accompanied with mitochondrial as well as lysosomal damage in the liver cells. The elevated level of NO, acted as an oxidative stressor, triggered cell death via p53 and MAPKAPK-2 signalling. Hence, NiO-NPs widespread application should be given meticulous attention for potential adverse biological effects.

Declaration of competing interest

The authors declare that they have no conflict of interest.

Acknowledgements

The authors are thankful to the Researchers Supporting Project number (RSP-2019/86), King Saud University, Riyadh, Saudi Arabia.

Appendix A. Supplementary data

Supplementary data to this article can be found online at https://doi.org/10.1016/j.chemosphere.2019.125488.

Author contribution statement

QS, PX conceived, designed and performed the experiments. QS and PX have equal contribution as first authors. QS and SMA characterized the nanoparticles. MAS performed the cytotoxicity measurements. MF, QS performed the immunofluorescence studies. AA Al-Alatar and MF performed the real time PCR experiments. QS and SMA performed the flow cytometric analysis. HAA did the ultra-sectioning of cells and performed electron microscopy studies. PX, JZ and YX performed the RNA-Seq experiments. AA Al-Khedhairy, XZ contributed reagent/materials and provide the necessary facilities. QS, PX also helped in data compilation and statistical analysis. QS, XZ wrote the article. QS, AA Al-Khedhairy, XZ discussed the results and made a critical revision of the manuscript.

References

Adeel, M., Ma, C., Ullah, S., Rizwan, M., Hao, Y., Chen, C., Jilani, G., Shakoor, N., Li, M., Wang, L., Tsang, D.C.W., Rinklebe, J., Rui, Y., Xing, B., 2019. Exposure to nickel oxide nanoparticles insinuates physiological, ultrastructural and oxidative damage: a life cycle study on Eisenia fetida. Environ. Pollut. 254, 113032.

Almeida, A., Bolanos, J.P., 2001. A transient inhibition of mitochondrial ATP synthesis by nitric oxide synthase activation triggered apoptosis in primary cortical neurons. J. Neurochem. 77, 676–690.

Bai, K.J., Chuang, K.J., Chen, J.K., Hua, H.E., Shen, Y.L., Liao, W.N., Lee, C.H., Chen, K.Y., Lee, K.Y., Hsiao, T.C., Pan, C.H., Ho, K.F., Chuang, H.C., 2018. Investigation into the pulmonary inflammopathology of exposure to nickel oxide nanoparticles in mice. Nanomedicine 14, 2329–2339.

Beaudrie, C.E.H., Kandlikar, M., Satterfield, T., 2013. From cradle-to-grave at the nanoscale: gaps in U.S. Regulatory oversight along the nanomaterial life cycle.

Environ. Sci. Technol. 47, 5524–5534.
Benej, M., Pastorekova, S., Pastorek, J., 2014. Carbonic anhydrase IX: regulation and role in cancer. Subcell. Biochem. 75, 199–219.
Bhaduri, G.A., Siller, L., 2013. Nickel nanoparticles catalyse reversible hydration of carbon dioxide for mineralization carbon capture and storage. Catalysis Science & Technology 3, 1234–1239.
Bonassi, S., Znaor, A., Ceppi, M., Lando, C., Chang, W.P., Holland, N., Kirsch-Volders, M., Zeiger, E., Ban, S., Barale, R., Bigatti, M.P., Bolognesi, C., Cebulska-Wasilewska, A., Fabianova, E., Fucic, A., Hagmar, L., Joksic, G., Martelli, A., Migliore, L., Mirkova, E., Scarfi, M.R., Zijno, A., Norppa, H., Fenech, M., 2007. An increased micronucleus frequency in peripheral blood lymphocytes predicts the risk of cancer in humans. Carcinogenesis 28, 625–631.
Cheng, G., Guo, W., Han, L., Chen, E., Kong, L., Wang, L., Ai, W., Song, N., Li, H., Chen, H., 2013. Cerium oxide nanoparticles induce cytotoxicity in human hepatoma SMMC-7721 cells via oxidative stress and the activation of MAPK signaling pathways. Toxicol. In Vitro 27, 1082–1088.
Dumala, N., Mangalampalli, B., Chinde, S., Kumari, S.I., Mahoob, M., Rahman, M.F., Grover, P., 2017. Genotoxicity study of nickel oxide nanoparticles in female Wistar rats after acute oral exposure. Mutagenesis 32, 417–427.
Epstein, C.B., Waddle, J.A., Hale, W., Davé, V., Thornton, J., Macatee, T.L., Garner, H.R., Butow, R.A., 2001. Genome-wide responses to mitochondrial dysfunction. Mol. Biol. Cell 12, 297–308.
Han, B., Li, W., Sun, Y., Zhou, L., Xu, Y., Zhao, X., 2014. A prolyl-hydroxylase inhibitor, ethyl-3,4-dihydroxybenzoate, induces cell autophagy and apoptosis in esophageal squamous cell carcinoma cells via up-regulation of BNIP3 and N-myc downstream-regulated gene-1. PLoS One 9, e107204.
Hirn, S., Semmler-Behnke, M., Schleh, C., Wenk, A., Lipka, J., Schaffler, M., Takenaka, S., Moller, W., Schmid, G., Simon, U., Kreyling, W.G., 2011. Particle size-dependent and surface charge-dependent biodistribution of gold nanoparticles after intravenous administration. Eur. J. Pharm. Biopharm. 77, 407–416.
Johnson, B.M., Fraietta, J.A., Gracias, D.T., Hope, J.L., Stairiker, C.J., Patel, P.R., Mueller, Y.M., McHugh, M.D., Jablonowski, L.J., Wheatley, M.A., Katsikis, P.D., 2015. Acute exposure to ZnO nanoparticles induces autophagic immune cell death. Nanotoxicology 9, 737–748.
Joy, A., Panicker, S., Shapiro, J.R., 2000. Altered nuclear localization of bax protein in BCNU-resistant glioma cells. J. Neuro Oncol. 49, 117–129.
Karamysheva, Z., Diaz-Martinez, L.A., Warrington, R., Yu, H., 2015. Graded requirement for the spliceosome in cell cycle progression. Cell Cycle 14, 1873–1883.
Kong, L., Hu, W., Lu, C., Cheng, K., Tang, M., 2019. Mechanisms underlying nickel nanoparticle induced reproductive toxicity and chemo-protective effects of vitamin C in male rats. Chemosphere 218, 259–265.
Korani, M., Rezayat, S.M., Gilani, K., Arbabi Bidgoli, S., Adeli, S., 2011. Acute and subchronic dermal toxicity of nanosilver in Guinea pig. Int. J. Nanomed. 6, 855–862.
Kruger, T., Scheer, U., 2010. p53 localizes to intranucleolar regions distinct from the ribosome production compartments. J. Cell Sci. 123, 1203–1208.
Lawrence, M., Huber, W., Pages, H., Aboyoun, P., Carlson, M., Gentleman, R., Morgan, M.T., Carey, V.J., 2013. Software for computing and annotating genomic ranges. PLoS Comput. Biol. 9, e1003118.
Lee, T.L., Raitano, J.M., Rennert, O.M., Chan, S.W., Chan, W.Y., 2012. Accessing the genomic effects of naked nanoceria in murine neuronal cells. Nanomedicine 8, 599–608.
Lee, Y., Kim, M., Han, J., Yeom, K.-H., Lee, S., Baek, S.H., Kim, V.N., 2004. MicroRNA genes are transcribed by RNA polymerase II. EMBO J. 23, 4051–4060.
Love, M.I., Huber, W., Anders, S., 2014. Moderated estimation of fold change and dispersion for RNA-seq data with DESeq2. Genome Biol. 15, 550.
Magaye, R., Gu, Y., Wang, Y., Su, H., Zhou, Q., Mao, G., Shi, H., Yue, X., Zou, B., Xu, J., Zhao, J., 2016. In vitro and in vivo evaluation of the toxicities induced by metallic nickel nano and fine particles. J. Mol. Histol. 47, 273–286.
Mirzayans, R., Andrais, B., Hansen, G., Murray, D., 2012. Role of in replicative senescence and DNA damage-induced premature senescence in p53-deficient human cells. Biochem. Res. Int. 8, 2012.
Mu, Y., Jia, D., He, Y., Miao, Y., Wu, H.-L., 2011. Nano nickel oxide modified non-enzymatic glucose sensors with enhanced sensitivity through an electrochemical process strategy at high potential. Biosens. Bioelectron. 26, 2948–2952.
Muhlfeld, C., Gehr, P., Rothen-Rutishauser, B., 2008. Translocation and cellular entering mechanisms of nanoparticles in the respiratory tract. Swiss Med. Wkly. 138, 387–391.
Murphy, M.P., 1999. Nitric oxide and cell death. Biochim. Biophys. Acta Bioenerg. 1411, 401–414.
Pietruska, J.R., Liu, X., Smith, A., McNeil, K., Weston, P., Zhitkovich, A., Hurt, R., Kane, A.B., 2011. Bioavailability, intracellular mobilization of nickel, and HIF-1 alpha activation in human lung epithelial cells exposed to metallic nickel and nickel oxide nanoparticles. Toxicol. Sci. 124, 138–148.
Porter, A.G., Janicke, R.U., 1999. Emerging roles of caspase-3 in apoptosis. Cell Death Differ. 6, 99–104.
Qian, F., He, M., Duan, W., Mao, L., Li, Q., Yu, Z., Zhou, Z., Zhang, Y., 2015. Cross regulation between hypoxia-inducible transcription factor-1α (HIF-1α) and transforming growth factor (TGF)-ß1 mediates nickel oxide nanoparticles (NiONPs)-induced pulmonary fibrosis. Am. J. Tourism Res. 7, 2364–2378.
Rao, K.V., Sunandana, C.S., 2008. Effect of fuel to oxidizer ratio on the structure, micro structure and EPR of combustion synthesized NiO nanoparticles. J. Nanosci. Nanotechnol. 8, 4247–4253.
Rasola, A., Bernardi, P., 2011. Mitochondrial permeability transition in Ca(2+)-dependent apoptosis and necrosis. Cell Calcium 50, 222–233.
Report on Carcinogens Fourteenth Edition, 2011. Nickel Compounds and Metallic Nickel.
Richter, C., Kass, G.E., 1991. Oxidative stress in mitochondria: its relationship to cellular Ca2+ homeostasis, cell death, proliferation, and differentiation. Chem. Biol. Interact. 77, 1–23.
Salimi, A., Sharifi, E., Noorbakhsh, A., Soltanian, S., 2007. Direct electrochemistry and electrocatalytic activity of catalase immobilized onto electrodeposited nanoscale islands of nickel oxide. Biophys. Chem. 125, 540–548.
Saquib, Q., Al-Khedhairy, A.A., Ahmad, J., Siddiqui, M.A., Dwivedi, S., Khan, S.T., Musarrat, J., 2013. Zinc ferrite nanoparticles activate IL-1b, NFKB1, CCL21 and NOS2 signaling to induce mitochondrial dependent intrinsic apoptotic pathway in WISH cells. Toxicol. Appl. Pharmacol. 273, 289–297.
Saquib, Q., Attia, S.M., Ansari, S.M., Al-Salim, A., Faisal, M., Alatar, A.A., Musarrat, J., Zhang, X., Al-Khedhairy, A.A., 2017. p53, MAPKAPK-2 and caspases regulate nickel oxide nanoparticles induce cell death and cytogenetic anomalies in rats. Int. J. Biol. Macromol. 105, 228–237.
Saquib, Q., Siddiqui, M.A., Ahmad, J., Ansari, S.M., Faisal, M., Wahab, R., Alatar, A.A., Al-Khedhairy, A.A., Musarrat, J., 2018. Nickel oxide nanoparticles induced transcriptomic alterations in HEPG2 cells. Adv. Exp. Med. Biol. 1048, 163–174.
Saquib, Q., Siddiqui, M.A., Ahmed, J., Al-Salim, A., Ansari, S.M., Faisal, M., Al-Khedhairy, A.A., Musarrat, J., AlWathnani, H.A., Alatar, A.A., Al-Arifi, S.A., 2016. Hazards of low dose flame-retardants (BDE-47 and BDE-32): influence on transcriptome regulation and cell death in human liver cells. J. Hazard Mater. 308, 37–49.
Schleh, C., Semmler-Behnke, M., Lipka, J., Wenk, A., Hirn, S., Schaffler, M., Schmid, G., Simon, U., Kreyling, W.G., 2012. Size and surface charge of gold nanoparticles determine absorption across intestinal barriers and accumulation in secondary target organs after oral administration. Nanotoxicology 6, 36–46.
Sebastian, C., Mostoslavsky, R., 2010. SIRT3 in calorie restriction: can you hear me now? Cell 143, 667–668.
Shah, A.N., Cadinu, D., Henke, R.M., Xin, X., Dastidar, R.G., Zhang, L., 2011. Deletion of a subgroup of ribosome-related genes minimizes hypoxia-induced changes and confers hypoxia tolerance. Physiol. Genom. 43, 855–872.
Sheikh, M.S., Fornace Jr., A.J., 2000. Role of p53 family members in apoptosis. J. Cell. Physiol. 182, 171–181.
Simpson, I.A., Dwyer, D., Malide, D., Moley, K.H., Travis, A., Vannucci, S.J., 2008. The facilitative glucose transporter GLUT3: 20 years of distinction. Am. J. Physiol. Endocrinol. Metab. 295, E242–E253.
Tiwari, D.K., Jin, T., Behari, J., 2011. Dose-dependent in-vivo toxicity assessment of silver nanoparticle in Wistar rats. Toxicol. Mech. Methods 21, 13–24.
Tracy, K., Macleod, K.F., 2007. Regulation of mitochondrial integrity, autophagy and cell survival by BNIP3. Autophagy 3, 616–619.
Trouiller, B., Reliene, R., Westbrook, A., Solaimani, P., Schiestl, R.H., 2009. Titanium dioxide nanoparticles induce DNA damage and genetic instability in vivo in mice. Cancer Res. 69, 8784–8789.
Valera, V.A., Walter, B.A., Linehan, W.M., Merino, M.J., 2011. Regulatory effects of microRNA-92 (miR-92) on VHL gene expression and the hypoxic activation of miR-210 in clear cell renal cell carcinoma. J. Cancer 2, 515–526.
Wiesner, M.R., Lowry, G.V., Alvarez, P., Dionysiou, D., Biswas, P., 2006. Assessing the risks of manufactured nanomaterials. Environ. Sci. Technol. 40, 4336–4345.
Wiseman, H., Halliwell, B., 1996. Damage to DNA by reactive oxygen and nitrogen species: role in inflammatory disease and progression to cancer. Biochem. J. 313 (Pt 1), 17–29.
Zhao, M., Antunes, F., Eaton, J.W., Brunk, U.T., 2003. Lysosomal enzymes promote mitochondrial oxidant production, cytochrome c release and apoptosis. Eur. J. Biochem. 270, 3778–3786.